Nanoscale

Accepted Manuscript

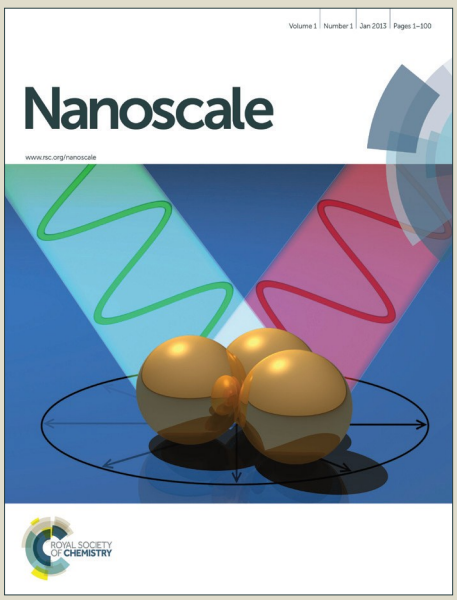

ROYAL SOCIETY OF CHEMISTRY

www.rsc.org/nanoscale

Journal Name

ARTICLE

Parametrization of Nanoparticles: Development of Full-particle Nanodescriptors

Received 00th January 20xx,
Accepted 00th January 20xx

DOI: 10.1039/x0xx00000x

www.rsc.org/

K. Tämm,[a*] L. Sikk,[a] J. Burk,[a] R. Rallo,[b] S. Pokhrel,[c] L. Mädler,[c] J. J. Scott-Fordsmand,[d] P. Burk,[a]

T. Tamm[e]

While metal oxide nanoparticles (NPs) are one of the most commonly used nanomaterials, the theoretical models used to analyze and predict their behavior have been mostly based on just the chemical composition or the extrapolation from small metal oxide clusters' calculations. In this study, a set of novel, theoretical full-particle descriptors for modeling, grouping or read-across of metal oxide NPs properties and biological activity was developed based on the force-field calculation of the potential energies of whole NPs. The capability of these nanodescriptors to describe biological activity was demonstrated over the Principal Component Analysis (PCA). The grouping provided by the PCA approach was found to be in good accordance with the algal growth inhibition data of well characterized nanoparticles, synthesized and measured inside the consortia of the EU 7FP framework MODERN project.

Introduction

Nanotechnology has successfully established itself in many areas of industry, and in fact, our everyday life. Several properties of nanoparticles (NPs), such as electromagnetic, catalytic, optical, mechanical etc. have been found to be significantly outperforming those of the respective materials in their bulk form. NPs are already routinely used in consumer products *i.e.* socks, solar protection, computer chips, food, etc. One the most interesting and challenging areas of NPs is their application in medicine, particularly for the diagnosis and treatment of human health issues. NPs are already used in medicine as biosensors and drug delivery agents,[1,2] and some progress in treatment of cancer has also been demonstrated.[3] Aside of many beneficial properties of NPs, their high bioactivity is often associated with toxic side effects. Most commonly, NPs enter the body through the inhalation route. Due to their small size, they are able to reach anywhere in the body, including entering various cell types and crossing the blood-brain barrier.[4] NPs also bind and carry heavy metals, which leads to cell damage.[4] One of the most studied side effects of NPs is the generation of oxidative stress in the body.[5,6,7] Under normal conditions, a body generates a small amount of reactive oxygen radicals (RORs) itself, and the enzymes and antioxidants in the body are able to defuse them very fast. In case of continuous inhalation of NPs, the quantity of RORs prevails and the defusing effect decreases, which in turn may cause airway inflammation and interstitial fibrosis.[4] Several studies have been carried out for obtaining information on nanotoxicity. Most of these studies have been based on EC_{50} measurements. Kahru and Dubourguier[8] compared the toxicities of NPs to the respective bulk materials and found that NPs have higher toxic effects to the environment. They also concluded that none of the seven NPs studied (TiO_2, CuO, ZnO, Ag, C_{60}-fullerene, single-walled carbon nanotubes, multi-walled carbon nanotubes) can be considered as non-toxic. Passagne *et.al.*[9] demonstrated the impact of size and relative surface area to toxicity. It was shown that the IC_{50} value for the 20 nm SiO_2 was 7 times smaller than for the same oxide particle of 100nm size. Similarly, both silver and gold NPs of smaller size were shown to be highly more toxic (via oxidative stress) than the respective larger (nano)particles.[10,11] Concurrently, Horie *et.al.*[12] studied the toxicities of 24 nano sized metal oxides and concluded that there is no remarkable impact of the size and surface area to the toxicity. These contradicting conclusions have been likely caused by different approaches as Passagne *et.al.*[9] compared the toxicities and surface areas for a single NP type, while Horie *et.al.* compared the ratio of surface area and toxicity of many different NPs. It has also been proposed that the toxicity is (mostly) caused by the release of metal ions from NPs into the cells. Comparing the results of different studies, one must bear in mind that NPs are a tricky target, they often have wide size distributions, they agglomerate even before reaching the culture media, upon which their surface adsorbs a variety of (bio)molecules from

[a]*Institute of Chemistry, University of Tartu, Ravila 14a, Tartu 50411, Estonia*
[b]*Dept Engn Informat & Matemat. Universitat Rovira i Virgili, Av. Paisos Catalans 26, Tarragona 43007, Spain*
[c]*Foundation Institute of Materials Science (IWT), Department of Production Engineering, University of Bremen, Germany*
[d]*Aarhus University, Dept Bioscience, Vejlsøvej 25, PO Box 314, 8600 Silkeborg, Denmark*
[e]*Institute of Technology, University of Tartu, Nooruse 1, Tartu 50411, Estonia*
* Corresponding author: karu@ut.ee
Electronic Supplementary Information (ESI) available:
[http://nano_descriptors.biocenit.cat

the environment, forming a "bio-corona". All these aspects make consistent bio-response experiments with NPs a challenge.

In parallel to *in vivo* and *in vitro* tests for the estimation of toxicities of NPs, *in silico* approaches have also been attempted. The most limiting factor for computational studies of NPs is, of course, their size. If a 5 nm NP contains approximately 20,000 atoms, then a 30 nm NP contains over 10 million atoms.[13] Therefore, due to the limits of computational resources, NPs cannot be adequately treated with conventional quantum mechanical methods. However, if some premises are applied, the (nano)QSARs (Quantitative Structure-Activity Relationships)[14,15] seem to be one of the most relevant methods for the prediction of toxicities or any other properties of NPs. For instance, Puzyn *et. al*.[16] developed a nanoQSAR model for the cytotoxicity of 17 metal oxide NPs to the bacteria *Escherichia coli*. The presumption was made that the toxicity is not affected by the size of the NPs (1.2 nm (12Å) NP were used throughout the modeling) and a correlation was established between the cytotoxicity and the metal cation heat of formation. Toropov *et. al*.[17] used so-called optimal molecular descriptors, which are considered as intermediaries between the classical and nanodescriptors, meaning that the descriptors can be calculated not only directly from the structure but also based on other information, which is related to the substance or to the experimental conditions. Toropov *et.* al.[17] modeled photo-induced cytotoxicity and dark cytotoxicity of NPs, the respective descriptors were obtained from SMILES-like codes. There have been also some other studies making use of the SMILES codes in the modelling.[18,19,20] NPs coated with organic molecules or some other metal atoms have been a subject of recent studies as the coating simplifies the transport of NPs to cells and reduces agglomeration. These kinds of particles have been also studied with QSAR[21] but with the presumption that all the properties of NPs depend solely on the molecular structure of the coating. It appears that the principal feature of nanomaterials – the high concentration of atoms (on the surface) with high potential energy – has not been adequately described numerically up to now.

The present work fills the gap in this research area by introducing and validating a set of newly developed full particle molecular descriptors which are calculated directly and solely from the structure of the respective NPs, not requiring external information apart from the crystal structure.

Computational details: Calculation of descriptors

Clearly, string-based approaches cannot provide the level of detail required to assess the energy differences of atoms on the surface of NPs and in the bulk, which is the foundation of the special properties of NPs. On the other hand, for quantum chemical methods, even the smallest NPs remain out of reach due to their sheer size. Therefore, force field based methods remain as the only viable option for all-atom approaches. By no means the only possible option, LAMMPS (Large-scale Atomic /Molecular Massively Parallel Simulator) software[22] was chosen for all calculations in the present work. The structures of NPs were derived from the thermodynamically most stable crystal structures of the respective bulk metal oxides. Unit cells of the metal oxides were replicated in all three dimensions by using the Moltemplate[23] software, and a spherical NP was generated by deleting all atoms outside of the set radius of the NP (see Figure 1), taking into account also the electroneutrality. Potential energies of atoms were calculated based on Buckingham potentials.[24] Coulombic interactions were calculated using Wolf summation,[25] a method computationally much more affordable than the Ewald summation.[26] Cutoff radii for the Wolf summation were derived from the modeling of an infinite crystal by periodic calculation of small clusters of unit cells (2x2x2 unit cells).

The derivation of nanodescriptors was based on the surface and shell model of the spherical NPs. In this framework, the NP is divided into the surface and shell regions (Figure 2), where the shell encompasses atoms that lie within 1 nm from the surface of the NP. This model allows the construction of a number of nanodescriptors, quantifying the special features of the surface atoms, based on the different computable parameters such as potential energies or coordination numbers. The calculations were performed with 3D periodic boundary conditions due to the requirements in the LAMMPS software.[22] The size of periodic box was much larger than the NP diameter and the cutoff values of Buckingham potentials and Wolf summation were selected to ensure that all atoms of NPs and interatomic interactions were contained within the box.

As the Buckingham potential parameters for Sb_2O_3 present in the datasets could not be found in the literature, they were derived from density functional theory calculations using the Gaussian 09 program package[27] at B3LYP//Def2-TZVPD[28,29] level. The relationship of potential energy to bond length was modeled by inflating the unit cell from 75% of experimental bond lengths to 200% bond lengths at 5% per step.

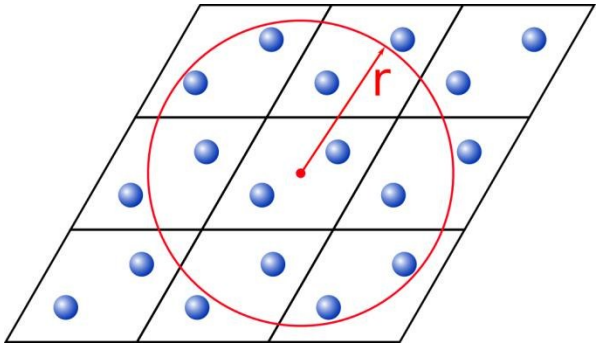

Fig. 1 Generation of spherical NPs from crystal structure.

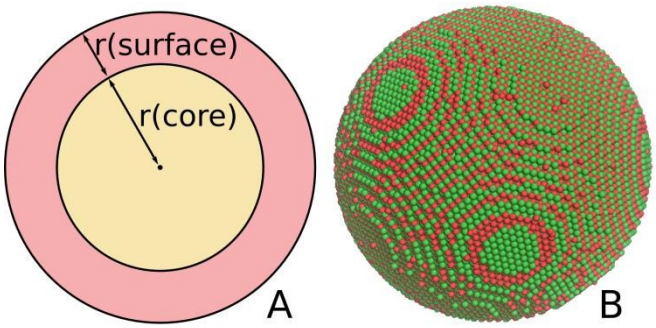

Fig. 2 The surface and shell regions of a NP (A); a NiO NP of 7 nm radius, as constructed for present work (B).

Results and Discussion

Based on the surface-core model, 35 individual nanodescriptors were constructed solely from the nanostructure itself. These descriptors were derived from the chemical composition (9), potential energy (9), lattice energy (5), topology (9) and size (3) (see Table 1 for classification of nanodescriptors and Table 2 with 35 descriptor values calculated for TiO_2 and Al_2O_3).

Constitutional descriptors hardly require any further explanations, as they are simply the counts of atoms of different identity and/or location. Since the range of descriptor values of this class is huge, log values can be used for QNAR development. Potential energy descriptors are also straightforward, derived from the force-field calculations, corresponding to the arithmetic means of the potential energies for specific atom types and/or locations in the NP. Lattice energies are based on the same potential energies but presented as per metal oxide nominal units (M_xO_y). All potential energy-related descriptors are presented in eV units. The coordination number of atoms is defined as the count of the neighboring atoms which lie inside the radius R

$$R=1.2*(R_M+R_O), \qquad (1)$$

where RM, RO are the ionic radii of metal and oxygen ions, respectively. The representatives of the last group of size-related descriptors were derived from the actual calculated NP diameter, obtained as the maximum separation (distance) between any two atoms in a NP. The formulae of all 35 descriptors are provided as Supplementary Information.

With a number of novel descriptors proposed that appear to have little differences in terms of their underlying features, the rightful question of inter-correlation arises. It would make sense to investigate the inter-correlations of the descriptors of the four main groups for some specific particle sizes rather than for some heterogeneous dataset. As expected, the pair-wise inter-correlations range from high ($R^2 > 0.99$) to very low ($R^2 < 0.0001$) values, with an overall average value of $R^2 = 0.24$. In order to obtain a structural overview, all pairwise inter-correlation among individual groups and between groups were investigated, the averaged inter-correlations are presented as

Table 1 Classification of descriptors calculated for metal oxide NPs.

Descriptor related to:	Basis of descriptor
Size	Diameter, surface area and volume of the NP in Å, Å^2, Å^3, respectively
Chemical composition (constitutional)	Total number of atoms in NP, in the surface and shell regions, metal and oxygen separately and together
Potential energy	Average potential energy of all atoms in NP, separately of metal atoms and oxygen atoms, in electron volts
Topology	Average coordination number of all atoms, metal atoms and oxygen atoms in the NP
Lattice energy	Lattice energy of the whole NP, the relative lattice energy (per diameter or per surface area or as compared to a perfect crystal) of the particle in electron volts

[1]Full list of descriptors for all NP used in this study is available in Supporting Information

a table (Table 3) for 10, 20, and 30 nm particles, the size group of descriptors had to be left out, for obvious reasons.

The inter-correlation table reveals some interesting details:

1) Inter-correlations among individual classes range from $R^2 = 0.47$ (potential energy, 20 nm) to $R^2 = 0.71$ (topological).

2) While inter-correlations among constitutional and topological classes are size-independent (as expected), potential energy related (including lattice energy) descriptors show some size-dependency.

3) Inter-correlations between different classes are very low, even for the seemingly related classes.

4) Inter-correlations between classes are more size dependent, surprisingly often the 20 nm size particles showing discrepancies.

Overall, according to the pair-wise inter-correlations, the four classes of 32 descriptors cover a large number of degrees of freedom, eliminating the suspicion of being just collinear variables with different names. The main advantages of these novel nanodescriptors over previously published descriptors for NPs can be summed as:

1) The descriptors are fully theoretical - based solely on the unit cell structure and Buckingham potential parameters, directly available for many compounds or derived from quantum chemical calculations.

2) The descriptors are inherently particle size dependent.

3) Overall inter-correlation among the descriptors is low.

4) The calculations are relatively simple technically and low cost computationally (the descriptors were calculated on dual-core G630@2.7GHz desktop PC).

5) Since the number of NPs of interest is not infinite (considering only spherical metal oxide NPs without functionalization), the descriptors can be pre-calculated for a range of NP sizes, allowing later use in swift QNAR construction for various endpoints. Optionally, a specific size/shape function for a descriptor can be constructed.

Table 2 Example of calculated descriptors for 11.57 nm TiO_2 and 11.4 nm Al_2O_3 NPs.

		TiO_2	Al_2O_3
Geometric:			
1	Diameter of the NP (Å)	115.7	114.00
2	Surface area of the NP (Å^2)*	42200.41	40828.13
3	Volume of the NP (Å^3)*	815171.39	775734.62
Constitutional:*			
4	Total number of atoms in NP*	78069	90805
5	Total number of atoms in surface region of NP*	44159	50860
6	Total number of atoms in shell region of NP*	33910	39945
7	Total number of metal atoms in NP*	26023	36322
8	Total number of metal atoms in surface region of NP*	14757	20354
9	Total number of metal atoms in shell region of NP*	11266	15968
10	Total number of oxygen atoms in NP*	52046	54483
11	Total number of oxygen atoms in surface region of NP*	29402	30506
12	Total number of oxygen atoms in shell region of NP*	22644	23977
Potential energy related:			
13	Average potential energy of all atoms in NP [eV]	-40.18	-31.95
14	Average potential energy of atoms in surface region of NP [eV]	-40.53	-32.20
15	Average potential energy of atoms in shell region of NP [eV]	-39.72	-31.64
16	Average potential energy of metal atoms in NP relative to infinite crystal [eV]	5.92E-001	3.42E-001
17	Average potential energy of metal atoms in surface region of NP relative to infinite crystal [eV]	8.03E-012	-3.14E-008
18	Average potential energy of metal atoms in shell region of NP relative to infinite crystal [eV]	1.37E+000	7.79E-001
19	Average potential energy of oxygen atoms in NP relative to infinite crystal [eV]	1.59E-001	1.70E-001
20	Average potential energy of oxygen atoms in surface region of NP relative to infinite crystal [eV]	-8.24E-004	9.24E-006
21	Average potential energy of oxygen atoms in shell region of NP relative to infinite crystal [eV]	3.67E-001	3.86E-001
Topologic:			
22	Average coordination number of all atoms in NP	3.90	4.68
23	Average coordination number of atoms in surface region of NP	4.00	4.80
24	Average coordination number of atoms in shell region of NP	3.77	4.53
25	Average coordination number of metal atoms in NP	5.84	5.85
26	Average coordination number of metal atoms in surface region of NP	6	6.00
27	Average coordination number of metal atoms in shell region of NP	5.64	5.65
28	Average coordination number of oxygen atoms in NP	2.93	3.90
29	Average coordination number of oxygen atoms in surface region of NP	3	4.00
30	Average coordination number of oxygen atoms in shell region of NP	2.84	3.77
Lattice energy related:			
31	Lattice energy of NP [eV]	-120.53	-159.77
32	Difference of the lattice energies of NP and infinite crystal [eV]	-0.91	-1.19
33	Lattice energy of NP divided by the diameter of NP [eV/Å]	-1.04	-1.40
34	Lattice energy of NP per unit surface area [eV/Å^2]*	-2.86E-03	-3.91E-03
35	Lattice energy of NP per unit volume [eV/Å^3]*	-1.48E-04	-2.06E-04

*Logarithmic values taken in modelling process

The capability of these nanodescriptors to capture the size dependency is paramount, as the main characteristic of NPs is the size, NPs with the same chemical composition but different size have been shown to possess different properties and toxicity values.[28] The size dependency of NP characteristics is typically non-linear and also saturates after reaching certain diameter. Therefore, size dependence has to be inherent to the individual descriptors and cannot be added as a correction term to a QNAR equation. To illustrate the different size-dependency behavior or different nanodescriptor classes, two descriptor value – NP size plots are presented in Figure 3.

As seen from the figure 3, both the shape of the size functions and the saturation or qualitative change regions vary significantly. The size dependence may be positive or negative, depending on the descriptor class and somewhat even on the individual descriptor. The qualitative change/saturation of size

Table 3. Average pairwise inter-correlations of nanodescriptors of four main classes for NPs of 10, 20 and 30 nm diameter.

	Constitutional			Potential energy			Topological			Lattice energy		
Size (nm)	10	20	30	10	20	30	10	20	30	10	20	30
Constitutional	0.65	0.65	0.65									
Potential energy	0.21	0.19	0.19	0.50	0.47	0.50						
Topological	0.04	0.04	0.04	0.11	0.10	0.10	0.71	0.71	0.71			
Lattice energy	0.09	0.09	0.09	0.26	0.24	0.25	0.06	0.06	0.06	0.61	0.61	0.59

dependence lies in the 10-20 nm NP radius range, depending on the descriptor class. Accordingly, a possible reason why some authors have claimed to see no relation to NP size in their experiments might be that they either have particles with diameters above the saturation limit or a wide size distribution for individual particles, effectively hiding the dependence. It is also clearly seen from Fig 3. that the special "nano" properties are in all cases most evident in the radius range of 5-30 nm, above that the properties resemble those of the bulk materials.

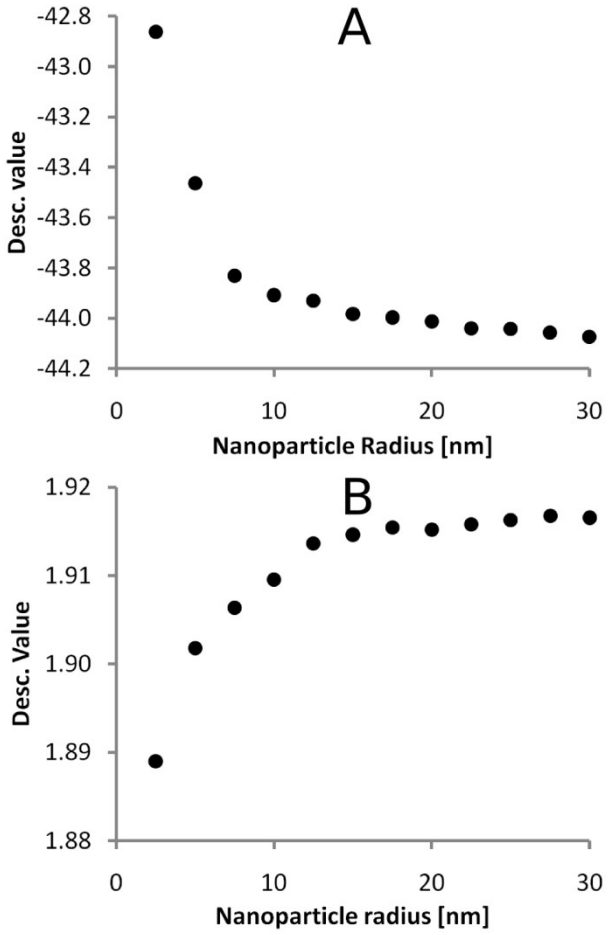

Fig. 3 Nanodescriptor values as a function of NP size for representatives of different descriptor classes: A) Potential energy (*Average potential energy of metal atoms in* Fe_2O_3); B) Topology (*Average coordination number of all oxygen atoms in* SiO_2).

While size itself may not be a parameter determining the particle activity, it has direct relation to the surface energy, which in turn determines the solubility of ions (often considered one of the main causes of metal oxide NP toxicity), the agglomeration tendency, and other key parameters of NPs.

Applicability of Nanodescriptors: Principal Component Analysis

The algal growth inhibition data of a rather special set of small and well described NPs from the work of Aruoja *et. al.*[30] , part of the EU 7FP MODERN, was analyzed with Principal Component Analysis (PCA) to find the relation between the experimental toxicities and the parameters represented by the descriptors. The original data set consisted of just 12 data points and Pd was further left out as it is not an oxide. As the small number of datapoints did not allow to use all descriptors in the PCA, a selection was made based on (low) intercorrelations to capture as much variance as possible. The summed results of the PCA are illustrated in Figure 4, with scores and loadings listed in Tables 4 and 5, respectively. The descriptors used in forming the principal components (PC) and algal growth inhibition experimental values for metal oxide NPs are given in Table 6. The analysis is complicated by the fact that in addition to the two fundamental factors (chemical identity and primary particle size), the agglomeration during the measurements influences the outcome.

This multitude of factors is reflected by the PCA results as well. The two shown (Figure 4) principal components describe 77% of the variance, and the three first PCs cover a significant 89%. The loadings of the PC1 appear to be mostly related to the "nano"-effect, as the main contributing descriptors - 101 and 407 – account for the size and active surface of the particles. As there is no direct correlation between the measured toxicity and the primary size across the chemically different particles, other factors need to be considered. PC2 is governed by the coordination number related descriptors of 309 and 306, but not as directly as was the case with PC1. With the contribution of the coordination number descriptors, this component accounts among other things also for the chemical bonding (ionic or covalent) in the NPs, in turn related to the potential toxicity mode *via* ion dissolution. Large negative scores would indicate covalently bound oxides, and hence, poor solubility.

Table 4 Experimental toxicity and **PCA** scores of the first three principal components for NPs.

NP	log(EC_{50})	PC 1	PC 2	PC 3
ZnO	-1.00	-3.008	-0.386	-0.173
CuO	-0.37	-1.844	-0.438	-0.125
Co_3O_4	0.05	1.723	0.804	-1.177
TiO_2	0.10	0.865	-0.329	1.099
Mn_3O_4	0.147	-0.321	0.404	-0.253
Fe_3O_4	0.30	1.235	2.422	-0.625
Al_2O_3	1.49	0.500	0.665	0.305
SiO_2	1.55	1.424	-1.577	-0.148
WO_3	1.76	2.088	-0.973	1.261
MgO	2.00	-2.16	1.378	0.981
Sb_2O_3	2.00	-0.501	-1.979	-1.136

Table 5 Loadings of the first three principal components.

Descriptor*	PC1	PC2	PC3
206	0.475	-0.344	0.323
407	0.535	0.046	-0.217
405	-0.453	-0.279	0.594
101	-0.459	0.016	-0.131
309	-0.142	0.720	-0.103
306	0.229	0.532	0.684

*See Table 6 for descriptor IDs

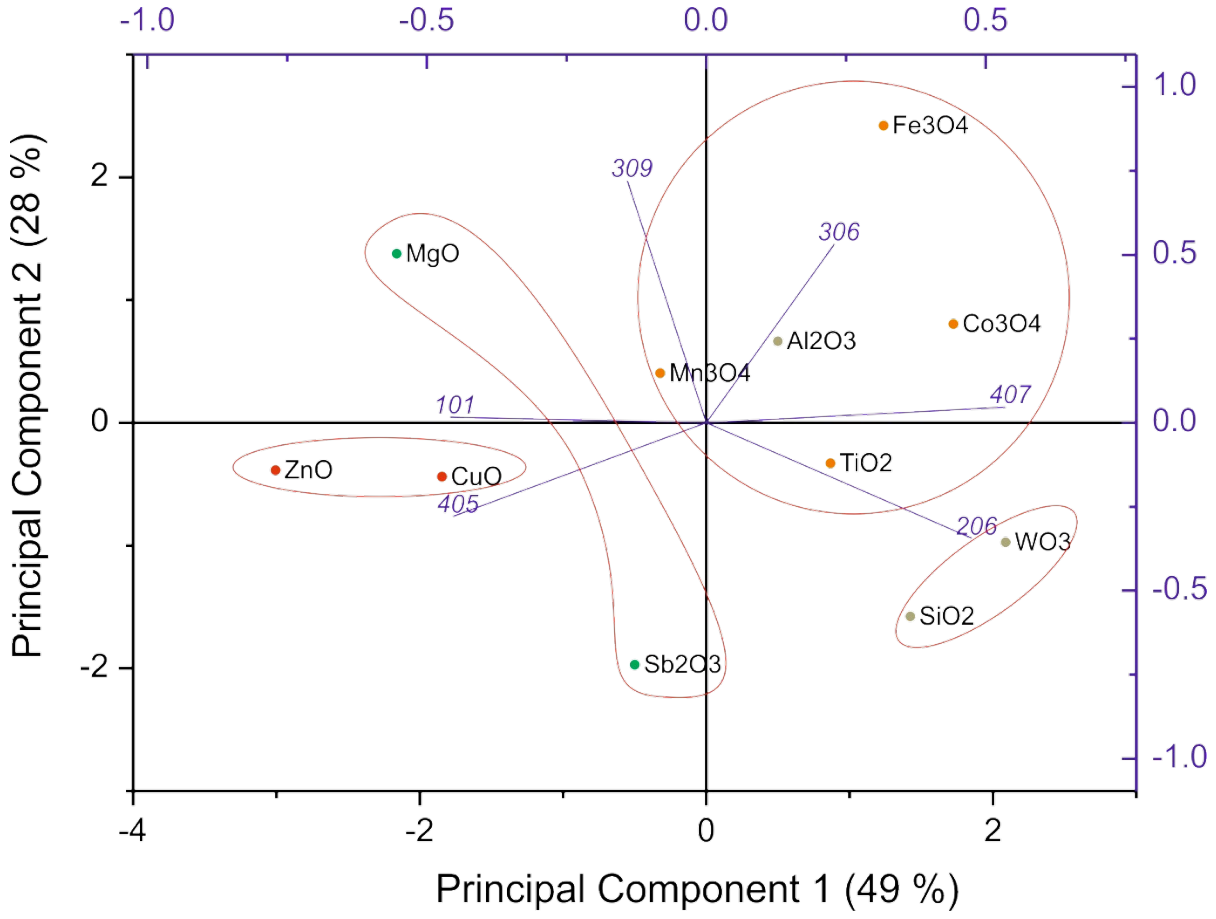

Fig. 4 Two-component PCA plot for 11 oxides with 6 descriptors used in the analysis. Toxicity scale from very toxic to non-toxic: red>orange>olive>green.

Considering the scores, as seen in Figure 4, all NPs are rather distributed, loosely forming groups in accordance with the experimental toxicities presented in Table 6. CuO and ZnO are forming a group as two of the most toxic oxides logEC_{50} values -0.37 and -1, respectively. The mainstream group is formed by the Al_2O_3, Co_3O_4, Fe_3O_4, Mn_3O_4 and TiO_2 (log EC_{50} 1.49, 0.05, 0.29, 0.13, 0.10). On this two-dimensional plot, Al_2O_3 would fit better to the group formed by SiO_2 and WO_3 (logEC_{50} 1.55 and

1.76 respectively), illustrating the fact that not all of the variance is covered by the two PCs. MgO and Sb_2O_3 form a detached group as their measured EC_{50} value was marked as >100, but the score values (see below) suggest different reasons for the low toxicity. These two compounds are poorly soluble, with Sb_2O_3 further possessing very limited ionic character.

A more detailed analysis of the score values for the three first principal components reveals certain trends. The most toxic group (CuO and ZnO) have high negative values for PC1 and moderately negative scores for PC2 and PC3. No other group shares the same distribution. There is one more particle with high negative PC1 (MgO), but in that case the scores of PC2 and PC3 are strongly positive, setting it apart. It can be concluded that the MgO nanoparticle would have potential of being toxic similarly to CuO and ZnO, according to potential energy on the surface, but its low solubility limits the dissolution and therefore toxic effect. The other least toxic particle Sb_2O_3 also differentiates from the rest, by moderately negative PC1 score and strongly negative PC2 and PC3 score. The rest of the less toxic particles (WO_3, SiO_2, Al_2O_3) are characterized by positive PC1 scores and positive or very slightly negative PC3 scores, with PC2 having either strongly positive or strongly negative scores. Therefore, for showing toxicity, moderately negative PC2 appears to be important, as positive and negative extremes lead to low toxicity.

In conclusion - in accordance with the complex nature of the experiments, the scores and loadings of the first three principal components need detailed analysis, as trends are not always clearly formed from high to low (or *vice versa*) values. Clearly, the toxic properties of a nanoparticle are governed by several parameters, which do not need to have extreme values, rather a certain optimal range is required.

To add more weight to our nanodescriptors, for testing purpose, we also re-modeled an already previously published nanoQSAR by Puzyn[16] and obtained a model with R^2=0.87, R^2_{cv} (or Q^2)=0.81. As the nanoQSAR is not an essence of this work, the details of this modeling approach are presented in Supplementary Information. The background of the QSAR method itself can be found elsewhere.[31,32]

Table 6. Experimental EC_{50}, NP sizes and descriptor values which were used for the principal component analysis.

			Descriptor ID					
	Log(EC$_{50}$)	***Dm* (nm)**	**101**	**206**	**306**	**309**	**405**	**407**
Al_2O_3	1.49	11.38	4.96	0.78	5.65	3.77	-1.19	-2.41
Co_3O_4	0.05	9.6	4.70	1.08	4.99	3.77	-2.10	-2.17
CuO	-0.37	12.2	4.97	-0.68	3.31	3.31	1.18	-3.06
Fe_3O_4	0.29	9.99	4.77	0.84	5.63	6.99	-2.00	-2.21
MgO	2	14.86	5.26	0.36	5.64	5.63	-0.24	-3.23
Mn_3O_4	0.13	17.41	5.39	0.68	5.02	3.77	-1.05	-2.72
Sb_2O_3	2	20.55	5.42	1.14	2.83	1.88	-0.96	-2.97
SiO_2	1.55	7.84	4.30	1.28	3.79	1.90	-1.10	-2.19
TiO_2	0.1	11.57	4.89	1.37	5.64	2.84	-0.91	-2.54
WO_3	1.76	10.56	4.67	1.71	5.65	1.88	-0.95	-2.23
ZnO	-1	20.37	5.47	0.17	3.86	3.86	-0.27	-3.52

101 Log of total number of atoms in NP.
206 Relative average potential energy of metal atoms in shell region of NP in electron volts.
306 Average coordination number of metal atoms in shell region of NP.
309 Average coordination number of oxygen atoms in shell region of NP.
405 Difference of the lattice energies of NP and infinite crystal.
407 Log of lattice energy of NP per unit surface area.

Conclusions

In the present work, a set of 35 novel full-particle descriptors – the first ever true nanodescriptors - was developed. While fully theoretical and computationally affordable, these descriptors can capture the essence of the very special NP properties and behaviour – their high concentration of active surface layer atoms. Nanodescriptors vary both with the size as well as with the chemical composition of the NPs. While appearing closely related at first glance, the pairwise intercorrelations of the nanodescriptors inter the classes and intra the classes remained outstandingly low, suggesting that a significant amount of variability in particle properties can be described with these descriptors. The validity of the nanodescriptors was demonstrated over the Principal Component Analysis (PCA) by using the experimental data measured within the EU 7FP framework MODERN. The analysis demonstrates the two and three principal components cover 77% and 89% of variance, respectively. The PCA scores group the particles in accordance with the experiment, while detailed analysis of both scores

and loadings can reveal important details of the toxicity mechanisms. The present approach neither includes specific electronic effects, nor was it attempted for mixed valence metal oxides or doped particles, however, these features can be added in the future, as more high quality experimental data becomes available to verify the performance of such additions. The descriptors developed in this study can be also used in parametrization of other inorganic NPs, such as quantum dots and NPs with non-spherical shape. In case of very small NPs, the use of semi-empirical methods should be considered as the electronic effect play crucial role in case of smaller NPs.

Acknowledgements

This material is based upon work supported by the EU Commission (MODERN, Contract no. 309314) and by the institutional research funding IUT (IUT20-15) of the Estonian Ministry of Education and Research. RR acknowledges the support received by Generalitat de Catalunya (2014-SGR1352). The authors are also thankful to Dr. Anne Kahru and Dr. Villem Aruoja for their contribution.

Notes and references

The values of the 35 nanodescriptors for 24 metal oxide NPs of 12 sizes between 5-60 nm, 10,080 values overall and the mathematical background for every descriptor and information on QNAR modeling are presented via Internet: www.ut.ee/cc/nano and nano_descriptors.biocenit.cat.

1. S. S. Agasti, S. Rana, M.-H. Park, C. K. Kim, C.-C. You and V. M. Rotello, *Adv. Drug Deliver Rev.*, 2010, **62**, 316.
2. W. H. De Jong and P. J. A. Borm, *Int. J. Nanomed.*, 2008, **3**, 133.
3. H. S. Huang and J. F. Hainfeld, *Int. J. Nanomed.*, 2013, **8**, 2521.
4. A. Nel, T. Xia, L. Madler and N. Li, *Science*, 2006, **311**, 622.
5. M. Horie, H. Kato, K. Fujita, S. Endoh and H. Iwahashi, *Chem. Res. Toxicol.*, 2012, **25**, 605.
6. T. Xia, M. Kovochich, M. Liong, L. Maedler, B. Gilbert, H. Shi, J. I. Yeh, J. I. Zink and A. E. Nel, *Acs Nano*, 2008, **2**, 2121.
7. A. Manke, L. Wang and Y. Rojanasakul, *BioMed Res. Int.*, 2013, **2013**, 942916-942916.
8. A. Kahru and H.-C. Dubourguier, *Toxicology*, 2010, **269**, 105.
9. I. Passagne, M. Morille, M. Rousset, I. Pujalte and B. L'Azou, *Toxicology*, 2012, **299**, 112.
10. A. Avalos, A. Isabel Haza, D. Mateo and P. Morales, *J. Appl. Toxicol.*, 2014, **34**, 413.
11. M. Misawa and J. Takahashi, *Nanomedicine*, 2011, **7**, 604.
12. M. Horie, K. Fujita, H. Kato, S. Endoh, K. Nishio, L. K. Komaba, A. Nakamura, A. Miyauchi, S. Kinugasa, Y. Hagihara, E. Niki, Y. Yoshida and H. Iwahashi, *Metallomics*, 2012, **4**, 350.
13. A. Gajewicz, B. Rasulev, T. C. Dinadayalane, P. Urbaszek, T. Puzyn, D. Leszczynska and J. Leszczynski, *Adv. Drug Deliv. Rev.*, 2012, **64**, 1663.
14. A. R. Katritzky, M. Kuanar, S. Slavov, C. D. Hall, M. Karelson, I. Kahn and D. A. Dobchev, *Chem. Rev.*, 2010, **110**, 5714.
15. A. Cherkasov, E. N. Muratov, D. Fourches, A. Varnek, I. I. Baskin, M. Cronin, J. Dearden, P. Gramatica, Y. C. Martin, R. Todeschini, V. Consonni, V. E. Kuz'min, R. Cramer, R. Benigni, C. Yang, J. Rathman, L. Terfloth, J. Gasteiger, A. Richard and A. Tropsha, *J. Med. Chem.*, 2014, **57**, 4977.
16. T. Puzyn, B. Rasulev, A. Gajewicz, X. Hu, T. P. Dasari, A. Michalkova, H.-M. Hwang, A. Toropov, D. Leszczynska and J. Leszczynski, *Nat. Nanotechnol.*, 2011, **6**, 175.
17. A. P. Toropova, A. A. Toropov, R. Rallo, D. Leszczynska and J. Leszczynski, *Ecotox. Environ. Safe.*, 2015, **112**, 39.
18. A. A. Toropov, A. P. Toropova, T. Puzyn, E. Benfenati, G. Gini, D. Leszczynska and J. Leszczynski, *Chemosphere*, 2013, **92**, 31.
19. T. Puzyn, D. Leszczynska and J. Leszczynski, *Small*, 2009, **5**, 2494.
20. A. A. Toropov, A. P. Toropova, E. Benfenati, G. Gini, T. Puzyn, D. Leszczynska and J. Leszczynski, *Chemosphere*, 2012, **89**, 1098.
21. S. Kar, A. Gajewicz, T. Puzyn and K. Roy, *Toxicol. in Vitro*, 2014, **28**, 600.
22. S. Plimpton, *J. Comput. Phys.*, 1995, **117**, 1.
23. A. Jewett and J. Lambert, www.moltemplate.org, (accessed April, 2016).
24. R. A. Buckingham, *P. Roy. Soc. Lond. A Mat.*, 1938, **168**, 264.
25. D. Wolf, P. Keblinski, S. R. Phillpot and J. Eggebrecht, *J. Chem. Phys.*, 1999, **110**, 8254.
26. P. P. Ewald, *Ann. Phys.*, 1921, **369**, 253.
27. M. J. Frisch, G. W. Trucks, H. B. Schlegel, G. E. Scuseria, M. A. Robb, J. R. Cheeseman, G. Scalmani, V. Barone, B. Mennucci, G. A. Petersson, H. Nakatsuji, M. Caricato, X. Li, H. P. Hratchian, A. F. Izmaylov, J. Bloino, G. Zheng, J. L. Sonnenberg, M. Hada, M. Ehara, K. Toyota, R. Fukuda, J. Hasegawa, M. Ishida, T. Nakajima, Y. Honda, O. Kitao, H. Nakai, T. Vreven, J. A. Montgomery Jr., J. E. Peralta, F. o. Ogliaro, M. J. Bearpark, J. Heyd, E. N. Brothers, K. N. Kudin, V. N. Staroverov, R. Kobayashi, J. Normand, K. Raghavachari, A. P. Rendell, J. C. Burant, S. S. Iyengar, J. Tomasi, M. Cossi, N. Rega, N. J. Millam, M. Klene, J. E. Knox, J. B. Cross, V. Bakken, C. Adamo, J. Jaramillo, R. Gomperts, R. E. Stratmann, O. Yazyev, A. J. Austin, R. Cammi, C. Pomelli, J. W. Ochterski, R. L. Martin, K. Morokuma, V. G. Zakrzewski, G. A. Voth, P. Salvador, J. J. Dannenberg, S. Dapprich, A. D. Daniels, Ć. d. n. Farkas, J. B. Foresman, J. V. Ortiz, J. Cioslowski and D. J. Fox, *Journal*, 2009.
28. A. D. Becke, *J. Chem. Phys.*, 1997, **107**, 8554.
29. D. Rappoport and F. Furche, *J. Chem. Phys.*, 2010, **133**, 134105.
30. V. Aruoja, S. Pokhrel, M. Sihtmaae, M. Mortimer, L. Maedler and A. Kahru, *Environ. Sci.: Nano*, 2015, **2**, 630.
31. J. Dearden, *IJQSPR.*, 2016, **1,** 1.
32. A. R. Katritzky, M. Kuanar, S. Slavov, C. D. Hall, M. Karelson, I. Kahn, D. A. Dobchev, *Chem. Rev.*, 2010, **110**, 5714.